PHYSICAL REVIEW VOLUME 161, NUMBER 2 10 SEPTEMBER 1967

Optical Detection of Spin-Lattice Relaxation and hfs in the Excited $\bar{E}(^2E)$ State of V^{2+} and Mn^{4+} in Al_2O_3

G. F. Imbusch, S. R. Chinn,* and S. Geschwind
Bell Telephone Laboratories, Murray Hill, New Jersey

(Received 23 February 1967)

The hyperfine structure (hfs) and spin-lattice relaxation in the excited $\bar{E}(^2E)$ states of V^{2+} and Mn^{4+} in Al_2O_3 have been studied by optical-detection techniques. This is an extension of an earlier study of EPR (electron paramagnetic resonance) in the excited $\bar{E}(^2E)$ state of Cr^{3+} in Al_2O_3. The experimental results for all three isoelectronic ions in the same host lattice allow us to make meaningful comparisons with theoretical ideas of hfs and spin-lattice relaxation. A well-resolved hfs is found for V^{2+} and Mn^{4+}, which is in contrast to the absence of hfs in the case of the isoelectronic Cr^{53} ion studied earlier. The values of the hyperfine-splitting parameter for the three ions can be adequately explained by considering the combined effects of the core-polarization hyperfine field, orbital hyperfine field, and dipolar hyperfine field. The experimental data are fitted to a simple spin Hamiltonian for an effective spin $S=\frac{1}{2}$ with $|g_{\parallel}|=2.2198\pm0.001$, and $|A_{\parallel}|=(46.3\pm1.5)\times10^{-4}$ cm^{-1} for V^{2+}, and $|g_{\parallel}|=3.0959\pm0.0006$, and $|A_{\parallel}|=(123\pm3)\times10^{-4}$ cm^{-1} for Mn^{4+}. Since $g_{\perp}\sim0$ for both ions, $A_{\perp}$ could not be determined. In the temperature range in which T_1 could be measured (1.4–2.15°K for V^{2+}, 6–9°K for Mn^{4+}), the spin-lattice relaxation times T_1 were found to follow an Orbach process: $T_1=c\exp(\Delta/kT)$, where Δ is the $2\bar{A}$-$\bar{E}$ splitting of the ^2E level. $\Delta=12.3$ and 80 cm^{-1} for V^{2+} and Mn^{4+}, respectively, and the measured values of c were 5.2×10^{-8} and 1.6×10^{-10} sec, respectively. For Cr^{3+}, where $\Delta=29$ cm^{-1}, the value of c, obtained earlier, is 3.8×10^{-9} sec. The parameter c is related to the direct-process relaxation time for the spontaneous transition between the non-time-reversed states $2\bar{A}$ and $\bar{E}$, $T_{2\bar{A}\to\bar{E}}$, in which a phonon of energy Δ is emitted. For the case where $\Delta\gg kT$, this direct-process relaxation time should vary inversely as $(V^{(1)})^2\Delta^3$, where $V^{(1)}$ is the orbit-lattice coupling parameter which can be determined from static-strain measurements, and the measured relaxation time is found to be so governed. In the vanadium experiment, the EPR signal was so weak that several new experimental techniques had to be used to extract the signal from the noise. In the case of manganese, a circular-polarization method to detect the excited-state EPR signal had to be developed. This technique of detecting excited-state EPR by monitoring circularly polarized light should be applicable to a wide variety of materials characterized by inhomogeneously broadened emission lines.

I. INTRODUCTION

Recent studies[1,2] of the EPR (electron paramagnetic resonance) in the $\bar{E}(^2E)$ excited state of Cr^{3+} in trigonal sites in Al_2O_3 have stimulated interest in applying the same optical detection techniques to examine the excited-state EPR of still other centers in solids. An obvious extension is to the study of the corresponding excited $\bar{E}(^2E)$ states of the isoelectronic $(3d)^3$ ions V^{2+} and Mn^{4+} in Al_2O_3,[3] and is described here. A study of EPR in the excited ^2E states of V^{2+} and Cr^{3+} in cubic sites in MgO has recently been reported.[4] The experimental results to be discussed here for the isoelectronic sequence, V^{2+}, Cr^{3+}, and Mn^{4+} in the same trigonal environment, provide a useful framework for a comparison with the theoretical ideas of hfs and spin-lattice relaxation. In the next section, the relevant crystal-field energy level diagram for these $(3d)^3$ ions is discussed with especial reference to the variation with ionic charge of the separation between some of the more pertinent energy levels. It is this variation that to a large extent is mainly responsible for the systematic differences among these ions that emerge in the hfs and spin-lattice relaxation. For example, it was found in the case of Cr^{3+} in Al_2O_3,[2] that in the liquid He temperature range, the spin-lattice relaxation time T_1 in the $\bar{E}(^2E)$ level proceeds via an Orbach process, i.e., $T_1=T_{2\bar{A}\to\bar{E}}e^{\Delta/kT}$. Here Δ is the separation between $2\bar{A}$ and $\bar{E}$ levels (see Fig. 1) and, since $\Delta\gg kT$, $T_{2\bar{A}\to\bar{E}}$ is the time for spontaneous decay from $2\bar{A}$ to $\bar{E}$ with emission of a phonon of frequency Δ. $T_{2\bar{A}\to\bar{E}}$ is essentially the time for a direct process between the *non*-time-reversed states $2\bar{A}$ and $\bar{E}$ and as $\Delta\gg kT$ it should vary inversely as Δ^3. As Δ varies from 12 to 80 cm^{-1} from V^{2+} to Mn^{4+}, one can check this Δ^3 dependence in the same crystal. Of course, appropriate account must be taken of the variation of the orbit-lattice coupling parameter among the three ions. This is done by reference to the change of the $2\bar{A}-\bar{E}$ level separation with static strain as will be discussed in Sec. V.

This series of $(3d)^3$ ions in corundum is also very useful in studying the systematics of hyperfine structure as one can observe the variation with nuclear charge in the same crystalline environment of the different contributions to the hyperfine field. The failure to observe a resolved hfs in the $\bar{E}(^2E)$ state of Cr^{3+} in Al_2O_3 was attributed to the accidental near cancellation

---

* Present address: Massachusetts Institute of Technology, Cambridge, Massachusetts.

[1] S. Geschwind, R. J. Collins, and A. L. Schawlow, Phys. Rev. Letters **3** 544 (1959).

[2] S. Geschwind, G. E. Devlin, R. L. Cohen, and S. R. Chinn, Phys. Rev. **137**, A1087 (1965).

[3] A very brief description of these results have been presented earlier: S. Chinn, G. E. Devlin, G. F. Imbusch, and S. Geschwind, Bull. Am. Phys. Soc. **10**, 56 (1965); G. F. Imbusch and S. Geschwind, Phys. Letters **18**, 109 (1965).

[4] L. L. Chase (to be published).

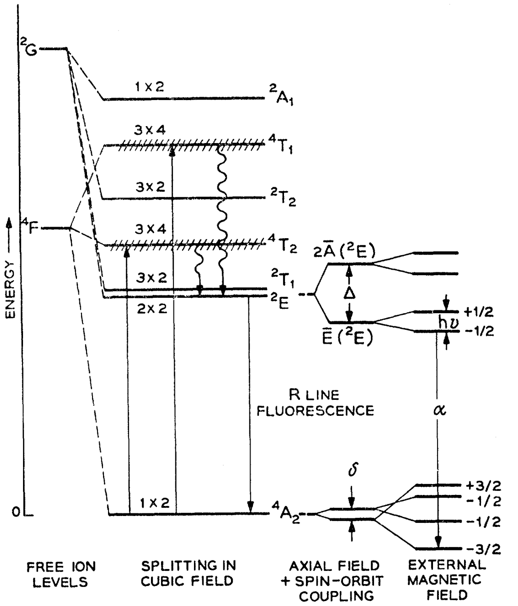

FIG. 1. Partial energy-level scheme for $(3d)^3$ ions in Al_2O_3. The Zeeman splittings of some of the levels with the magnetic field parallel to the c axis are also shown (not to scale).

of the core-polarization hyperfine field (cphf) with the orbital hyperfine field.[2] The cphf is essentially constant for the isoelectronic sequence,[5] however, the orbital hyperfine field is proportional to the g shift which is quite different for each of these three ions and a well-resolved hfs structure is indeed observed in V^{2+} and Mn^{4+} as will be described in Sec. IV.

In the optical detection of EPR, one makes use of the fact that when one microwave photon is absorbed in the excited state, some aspect of the fluorescence pattern changes by the amount of one optical photon. Thus the detection of EPR is removed from the realm of the detection of microwave photons to the much more sensitive region of detecting optical photons. This is the analog in solids of the optical rf double-resonance techniques first suggested by Brossel and Kastler[6] and widely used in gases as, for example, first applied by Brossel and Bitter[7] to the $^3P_1$ levels of mercury. Three distinct techniques of optical detection of excited-state EPR in solids have been previously outlined.[2] The methods of selective reabsorption[1] and the use of a high-resolution optical spectrometer have been previously realized experimentally and can only be used for optical lines which are sharp compared to Zeeman splittings. The third method, which makes use of the circular polarization of the fluorescent light, is applicable to broad emission lines as well and had to be developed for the first time in a solid for Al_2O_3:Mn^{4+} which has optical linewidths of several cm^{-1}, as described in Sec. III D. In the case of Al_2O_3:V^{2+}, the emission lines were a fraction of a cm^{-1} in width, so that a high-resolution optical spectrometer could be used as in the case of Al_2O_3:Cr^{3+} previously reported.[2] Nonetheless, the vanadium signal was so weak that several new experimental techniques had to be used to extract the very weak signals from the noise. All these experimental details are fully treated in Sec. III.

II. ENERGY LEVEL SCHEME OF $(3d)^3$ IONS IN AL_2O_3

In Al_2O_3 each of the $(3d)^3$ ions in question enters substitutionally for the Al^{3+}. The Al^{3+} ion is octahedrally coordinated by 6 oxygen ions giving rise to a predominantly cubic crystalline electric field. The octahedron is trigonally distorted with resultant site symmetry C_3. The crystal-field splitting of Cr^{3+} in Al_2O_3 was first treated in detail by Sugano and Tanabe[8] and their analysis is, in the main, applicable to V^{2+} and Mn^{4+} in Al_2O_3 as well, with the appropriate change in the magnitude of certain crystal-field parameters and the spin-orbit coupling. In both the case of V^{2+} and Mn^{4+} it is believed that the necessary charge compensation is nonlocal. In any event the local C_3 symmetry is preserved. Referring to Fig. 1, the free-ion ground state of $(3d)^3$ is ^4F, which splits in a cubic field into the $^4A_2$ ground state and into the two orbital triplets $^4T_2$ and $^4T_1$ shown by cross hatching. The well-known excited-state ^2E level originates from the free-ion ^2G level. The combination of the trigonal field and spin-orbit coupling splits the ^2E level into two Kramers doublets separated by an energy Δ and it is in the lower of these doublets, i.e., the $\bar{E}(^2E)$, that EPR is performed. A steady-state population is maintained in $\bar{E}(^2E)$ by continuous pumping with broadband light into the $^4T_2$ and $^4T_1$ bands from which the ions decay by rapid nonradiative multiphonon processes to the $\bar{E}$ level. The $\bar{E}$ level decays to the ground state by fluorescence.

The positions of the most pertinent energy levels and the radiative lifetime of $\bar{E}$ for the three ions are listed in Table I. It is apparent that there is a systematic variation, along the isoelectronic series, of level spacings and radiative lifetimes. First one notes that the cubic crystal-field splitting $10Dq$, which is roughly measured by the energy of the $^4T_2$ level, increases with ionic charge. This increase of $10Dq$ with charge in the same environment is well known empirically and is discussed by McClure.[8] The ^2E splitting Δ is given by Sugano and Tanabe[9] as

$$\Delta = 4K\zeta/[W(^2E) - W(^2T_2)], \qquad (1)$$

where K measures the strength of the trigonal field and ζ is the one-electron spin-orbit coupling parameter. The free-ion value of ζ increases from 168 cm^{-1} to $\sim$410

---

[5] S. Geschwind, J. Appl. Phys. **36**, 920 (1965).

[6] J. Brossel and A. Kastler, Compt. Rend. **229**, 1213 (1949).

[7] J. Brossel and F. Bitter, Phys. Rev. **86**, 308 (1952).

[8] D. S. McClure, in *Solid State Physics*, edited by F. Seitz and D. Turnbull (Academic Press Inc., New York, 1959), Vol. 9, Table VII.

[9] S. Sugano and Y. Tanabe, J. Phys. Soc. Japan **13**, 880 (1958).

Table I. Energy levels,[a] splittings, and radiative lifetimes for the three ions in Al_2O_3. The energies are in cm^{-1} and the radiative lifetimes were measured at 4.2°K.

Ion	$\bar{E}(^2E)$	$^2T_1$	$^2T_2$	$^4T_2$	$^4T_1$	^2E splitting $\Delta(cm^{-1})$	Ground-state splitting (cm^{-1})	Radiative lifetime of $\bar{E}(^2E)$ (msec)
V^{2+} [b]	11 679.2		∼17 000	15 200	21 500	12.3	0.33	65
Cr^{3+} [c,d]	14 417.7	15 050	21 000	18 000	25 000	29	0.38	3.5
Mn^{4+} [e–g]	14 781.7	∼15 500	∼21 200	20 800	∼25 000	80	0.39	0.83

[a] Positions of levels are referred to $^4A_2$ ground state.
[b] M. D. Sturge, Phys. Rev. **130**, 639 (1963).
[c] S. Sugano and I. Tsujikawa, J. Phys. Soc. Japan **13**, 899 (1958).
[d] D. F. Nelson and M. D. Sturge, Phys. Rev. **137**, A1117 (1965).
[e] S. Geschwind, P. Kisliuk, M. P. Klein, J. P. Remeika, and D. L. Wood, Phys. Rev. **126**, 1684 (1962).
[f] M. Crozier, Phys. Letters **18**, 219 (1965).
[g] Present work.

cm^{-1} in going from V^{2+} to Mn^{4+}.[10] This increase by itself is not large enough to explain the observed increase in Δ. One is, therefore, led to postulate that K increases as well by approximately a factor of 2.5. This increase of K is also consistent with the g shift in the $\bar{E}$ state whose largest term,[11] to a good approximation within the same crystal-field framework as that used to obtain Eq. (1), is given by

$$\Delta g = \frac{12K^2}{[W(^2E)-W(^2T_2)][W(^2E)-W(^2T_1)]}. \quad (2)$$

Since it is seen from Table I that the energy denominators in Eq. (2) are almost the same for all the ions, we would expect $\Delta g \sim K^2$ and this is what is roughly observed. ζ is, of course, reduced in the crystal below its free-ion value. One finds that a reasonably good fit to Δ and Δg for V^{2+}, Cr^{3+}, and Mn^{4+} is had by choosing $\zeta = 100$, 170, and 230 cm^{-1}, respectively, and $K = -175$, -300, -450 cm^{-1}, respectively. Effects of orbital reduction have been omitted and absorbed into these values. We do not mean for these values to be taken too literally but cite them as being at least illustrative of the qualitative trend of K. We offer no theoretical reason for the increase in the trigonal field. [*Note added in proof.* Calculations of g parameters for the ^2E levels of Cr^{3+} systems have been made by Macfarlane (unpublished) in terms of the v and v' parameters, where

$$v = \tfrac{3}{2}\langle t_{20} | V(T_2) | t_{20}\rangle = -3K$$

and

$$v' = \langle t_{2+} | V(T_2) | e_{+}\rangle.$$

A better agreement for g parameters is obtained by use of this two-parameter calculation but our one-parameter model is adequate for this discussion. One important point from Macfarlane's work is that the additional perturbation loops obtained by the use of v' contribute only to the orbital g shift consistent with the assumption used later that $g_{\parallel}-2$ is a measure of the orbital g shift.]

Finally, it is interesting to note the systematic decrease in the radiative lifetime τ_R from V^{2+} to Mn^{4+} which is indicative of increasing oscillator strength of the ^2E fluorescence. As this oscillator strength is borrowed from the absorption bands,[9] it implies much weaker absorption bands for the V^{2+} than the Mn^{4+}. This weaker absorption of the exciting light in V^{2+}, in combination with other factors described in Sec. III, resulted in considerably lower population of V^{2+} ions in the $\bar{E}$ state compared to Cr^{3+} and Mn^{4+} and consequently much weaker magnetic resonance signals.

When an external magnetic field $\mathbf{H}_0$ is applied parallel to the c axis, the resultant Zeeman splitting is as shown in Fig. 2.[9] The σ selection rules hold when the fluorescence is viewed at right angles to the c axis and when the radiation is polarized with the electric vector $\mathbf{E}$ perpendicular to the c axis. The circular polarization rules hold with the light viewed along the c axis with $\mathbf{H}_0 \parallel \mathbf{c}$. Microwave resonance in the $\bar{E}$ state of V^{2+} is observed by monitoring a change in fluorescent intensity of a particular Zeeman component with a high-resolution optical spectrometer as was done in ruby.[2] For Mn^{4+} the fluorescent lines are too broad to be resolved in normal laboratory fields so that magnetic resonance is detected by monitoring a change in circularly polarized fluorescence[3] of a particular sense as will be described more fully in the next section.

III. EXPERIMENTAL PROCEDURE

A. General Outline

Three methods of optical detection of microwave absorption in excited states have been outlined in Ref. 2. The general principle of optical detection is easily illustrated with reference to Fig. 2. Assume that there is rapid thermalization between the Zeeman levels of $\bar{E}$, so that at low temperature the lower Zeeman level $(u_{+}-\frac{1}{2})$ is more heavily populated or that some other mechanism of selectively populating the lower level is operative.[12] The fluorescent intensity from this level will therefore be stronger than from the upper level. When

---

[10] See Table VIII in Ref. 8.

[11] The complete expression for g in the $\bar{E}(^2E)$ and $2\bar{A}(^2E)$ states of $(3d)^3$ ions in the trigonal crystal field of corundum is given in Ref. 9.

[12] G. F. Imbusch and S. Geschwind, Phys. Rev. Letters **17**, 238 (1966).

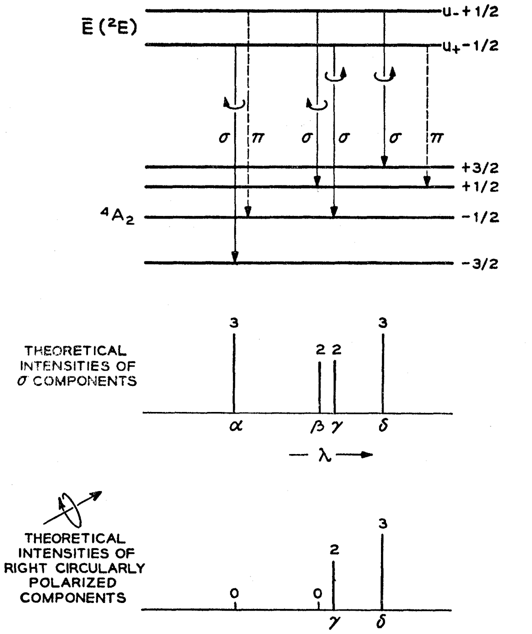

FIG. 2. Selection rules for the $\bar{E}(^2E)\rightarrow{}^4A_2$ transitions (Zeeman components of the R_1 line) of $(3d)^3$ ions in Al_2O_3. The magnetic field is applied parallel to the c axis. The linear selection rules hold when light is viewed in a direction at right angles to the c axis. The circular-polarization selection rules hold when light is viewed along the direction of the magnetic field. The π transitions (shown as dashed lines) are usually weak and can be neglected.

microwave energy at a frequency corresponding to the Zeeman splitting of $\bar{E}$ impinges on the crystal, transitions are induced which decrease the population in the $(u_+-\frac{1}{2})$ level so that the fluorescent intensity originating in this level is reduced while that from the $(u_-+\frac{1}{2})$ level is increased. Experimentally, then, we look for a method to preferentially detect fluorescence from one of these levels. When the optical emission lines are sufficiently sharp compared to the Zeeman splitting, a high-resolution spectrometer can be used to monitor an individual optical Zeeman component, such as α. When microwave absorption occurs, the α intensity decreases. This method was used for V^{2+}. In Al_2O_3:Mn^{4+}, however, the fluorescence linewidth is $\sim$4 cm^{-1} so that the Zeeman splitting in $\bar{E}$ cannot be resolved optically. In this case, the circular-polarization method can be used. From the selection rules in Fig. 2, it is seen that more right circularly polarized light comes from $(u_-+\frac{1}{2})$ as compared with $(u_+-\frac{1}{2})$. Magnetic resonance in $\bar{E}$ will therefore result in an increase in the intensity of right circularly polarized light. In this detection scheme a circular-polarization analyzer (quarter-wave plate and linear polarizer) replaces the high-resolution spectrometer. This latter method is, of course, more nearly identical to the optical rf double resonance in gases. The general experimental arrangement is illustrated in Fig. 3. The single-crystal sample, in the form of an elongated rectangular prism, was mounted with its long axis vertical and along the axis of TE_{012} microwave cavity. The c axis of the crystal was along one of the two smaller dimensions of the specimen and generally parallel to the magnetic field. The cavity was placed in a flat-bottomed helium cryostat made of glass whose lower portion was unsilvered. The sample was continuously illuminated vertically from below by a 200-W mercury or mercury-xenon lamp through a small hole cut in the base of the cavity. Broadband optical filters were used to remove infrared radiation from the pumping light as well as to select radiation to match the absorption bands of the samples. The fluorescent light was observed through horizontal slits cut in the side wall of the cavity in such a way as not to interfere with the microwave current flow. The experiments were performed at 24 and 48 kMc/sec in a temperature range from 1.5 to 10°K. Below 4.2°K, the cavity and sample were in contact with the liquid He and temperature was measured by monitoring the He vapor pressure. Special precautions had to be taken to ensure that the pumping light did not significantly raise the sample temperature above that of the bath. Temperatures above 4.2°K were reached by blowing cold He gas, obtained by boil-off from a liquid-helium reservoir in a standard container, over the microwave

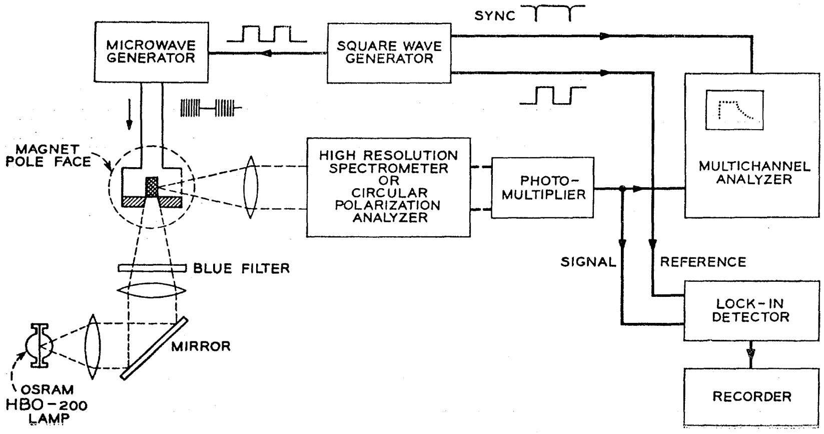

FIG. 3. Block diagram of apparatus used for optical detection of EPR in metastable excited states.

cavity and sample. By means of a small heater placed at the exit of the gas transfer tube, the sample temperature could be varied from approximately 5°K upward. The temperature was monitored by means of a small carbon resistor attached to the cavity. Independent checks indicated no significant difference between the sample and cavity temperature. A temperature stabilization unit, using the carbon resistor as the sensing element, controlled the heat supplied to the heating coil to keep the sample temperature constant. This unit, designed by M. Graifman, will be more fully described elsewhere.[13]

Each of the two optical detection techniques that were used posed its own set of experimental problems. The experimental details for these two ions will therefore be separately discussed in Secs. III C and III D following a description of the sample preparation.

B. Sample Preparation

When vanadium is substituted for aluminum in Al_2O_3, it enters as V^{3+}. Gamma irradiation over a period of several hours converts a small fraction of the V^{3+} ions to V^{2+} so that a detectable optical fluorescence signal from $Al_2O_3:V^{2+}$ can be observed.[14] The difficulty in obtaining a sufficiently large density of V^{2+} ions and the relative weakness of the vanadium optical transition probabilities mean weak fluorescence intensity and this makes the detection of EPR in the vanadium excited state a difficult task. The vanadium fluorescence lines are of comparable sharpness with the fluorescence lines from good quality ruby crystals, i.e., approximately $0.1\sim 0.2$ cm^{-1}.

Al_2O_3 doped with Mn^{4+} can be grown by providing charge compensation in the form of Mg^{2+} ions.[15] Maximum concentrations of Mn^{4+} approaching 0.3% can be obtained in this manner. Further, the fast radiative decay rate is indicative of strong optical transition probabilities and consequently intense red fluorescence is observed from $Al_2O_3:Mn^{4+}$. In contrast to the case of V^{2+} and Cr^{3+} the Zeeman splitting is not completely resolved with magnetic fields obtainable from conventional electromagnets. Crozier[16] has resolved the Zeeman splitting by applying fields of up to 100 000 G and the linear polarization selection rules appear to be roughly obeyed.

The samples were cut in the form of rectangular prisms of approximate dimensions $0.3\times 0.1\times 0.1$ in. for K band work and $0.16\times 0.06\times 0.06$ in. for 48-kMc/sec work. The c axis was parallel to one of the shorter axes.

C. V^{2+} in Al_2O_3

1. *Estimate of Signal-to-Noise Ratio* (S/N)

The vanadium experiments were performed mainly at K band (0.8 cm^{-1}) at which frequency, the thermal equilibrium population ratio at 1.5°K for the Zeeman components of $\bar{E}$ should be 2:1. If the populations of the two levels of $\bar{E}$ are made equal, the intensity of the α fluorescent component will decrease by 25%. The V^{51} isotope (99% abundant) has a spin of $\frac{7}{2}$ which should give rise to an 8-line hyperfine pattern. When resonance occurs at one of these hyperfine components, $\frac{1}{8}$ of the ions can absorb microwave power and if this power is sufficient to equalize populations for this particular m_I transition, the intensity of α will decrease by around 3%. Actually only a $\frac{1}{2}$% change in α intensity was observed. This reduced value of signal was probably due to incomplete saturation of the microwave line due to the very small value of $g_\perp$. There was also strong evidence that a hole was being burned in an inhomogeneously broadened microwave line. This could easily occur and the small value of $g_\perp$ would impede spin diffusion between the spin packets in the line.

The observation of this $\frac{1}{2}$% EPR light signal was made difficult by the relatively large shot-noise in the weak fluorescent light signal. Even with the largest possible slit width in the optical spectrometer, consistent with resolving the Zeeman components in the $\bar{E}$ state, only 2×10^5 photon/sec were registered by the photomultiplier. The fractional shot-noise in this registered light flux is $1/(2\times 10^5)^{1/2}$ or approximately 0.2%. Thus to get a reasonable signal-to-noise ratio, one would need an integration time, or time constant of the system, of approximately 10 sec. To reproduce the anticipated 8-line hyperfine pattern without distortion and reasonable S/N would then require sweeping through the pattern in a time of the order of an hour. Slow drifts in the apparatus make it unfeasible to use a lock-in detector over such a long time and in practice it was found that it was not possible to obtain a satisfactory signal for V^{2+} by using lock-in detection. Instead, a continuous averaging technique had to be used.[2,17]

2. *Use of Continuous Averaging to Record the EPR Pattern*

With the microwave power continuously applied, the external magnetic field was swept through the entire magnetic resonance pattern as the analyzer, operating in a time mode, swept through its 400 channels. Thus, during one such sweep, each channel recorded a number of pulses corresponding to the fluorescent light intensity at the value of the magnetic field at the time that

---

[13] M. B. Graifman (to be published).

[14] M. D. Sturge, Phys. Rev. **130**, 639 (1963).

[15] S. Geschwind, P. Kisliuk, M. P. Klein, J. P. Remeika, and D. L. Wood, in *Proceedings of the International Conference on Paramagnetic Resonance, Jerusalem, 1962*, edited by W. Low (Academic Press Inc., New York, 1964), p. 113; Phys. Rev. **126**, 1684 (1962).

[16] M. H. Crozier, Phys. Letters **18**, 219 (1965).

[17] M. P. Klein and G. W. Barton, Jr., in *Proceedings of the International Conference on Paramagnetic Resonance, Jeruaslem, 1962*, edited by W. Low (Academic Press Inc., New York, 1964), p. 698; Rev. Sci. Instr. **34**, 754 (1963).

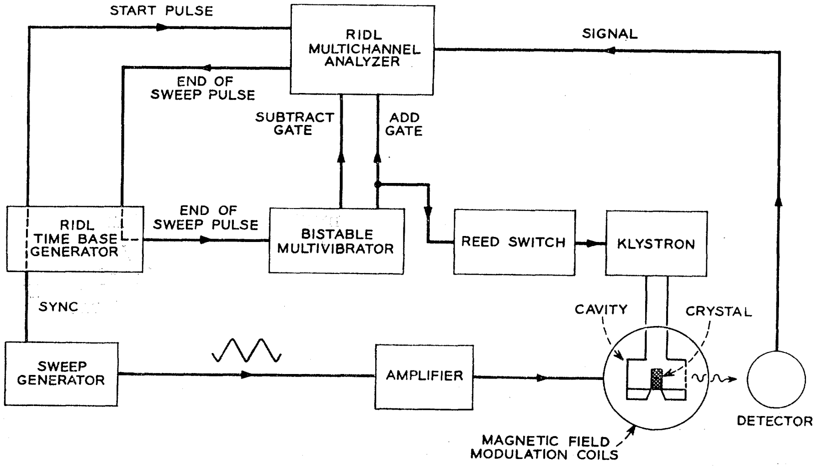

FIG. 4. Block diagram of system used for the observation of the hfs in the excited state of V^{2+} in Al_2O_3. A periodic sweep voltage from the generator causes the magnetic field to sweep twice (upward and downward) through the resonance during each period. The photon pulses constituting the optical signal are registered by the multichannel analyzer, one sweep of which corresponds approximately to one period of the sweep generator. The analyzer is triggered into *add* and *subtract* modes on alternate sweeps, while the microwave power is applied only during the *add* cycle. See Fig. 5 and text.

particular channel was open. The analyzer sweep and field sweep were synchronized so that each channel corresponded to the same value of magnetic field on repeated sweeps. During a typical run, the dwell time on each channel was 1.25 msec so that the time for a complete single sweep was 0.5 sec. We saw above, that with the recorded light flux of 2×10^5 photon/sec an integration time of 10 sec was desirable to obtain a reasonable S/N ratio in the face of the shot noise. To obtain this 10-sec integration time at a 1.25-msec channel width, 8000 sweeps were necessary or a running time of 4000 sec, i.e., over 1h. If the noise were all white noise, there would, of course, be no fundamental advantage in using the method of continuous averaging as compared to the more ordinary lock-in detection. As described in this application, both schemes have the same time constant of 10 sec, determined for the lock-in detector by an RC network and for the analyzer by the total counting time per channel. However, one does not have a white-noise spectrum but must contend with slow drifts in experimental conditions and $1/f$ noise and it is this type of noise which is overcome by the method of continuous averaging.

In addition to the random noise just discussed, there is an additional unwanted background connected with the magnetic field sweep and use of a high-resolution spectrometer that will now be described. The full hyperfine pattern of V^{2+} extends over a region of 350 G so that a ±200 G magnetic field modulation is necessary for its display. However, the wavelength of the particular Zeeman transition being monitored varies with magnetic field. Consequently, with the spectrometer tuned to a fixed wavelength, this field modulation moves the peak of the optical line and produces a field-dependent change in detected light in addition to the EPR signal.

To estimate the size of this unwanted signal let us assume a Gaussian-shaped optical line with peak intensity normalized to unity. The intensity at a distance $\Delta\nu$ cm^{-1} from the peak is given by

$$I(\Delta\nu)=\exp[-\ln2(\Delta\nu/\delta)^2], \tag{3}$$

where 2δ is the full width of the line at half-maximum. The size of the field modulation is such that one may assume $\Delta\nu/\delta$ is small, so that

$$I(\Delta\nu)\sim1-\ln2(\Delta\nu/\delta)^2. \tag{4}$$

The α transition occurs between $\bar{E}(-\frac{1}{2})$ and $^4A_2(-\frac{3}{2})$, and if g' and g'' denote the values of g in the $\bar{E}$ and $^4A_2$ states, respectively, then the shift in the peak of the α line $\Delta\nu_\alpha$, when the magnetic field varies by ΔH, is given by

$$hc(\Delta\nu_\alpha)=(\tfrac{3}{2}g''-\tfrac{1}{2}g')\beta\Delta H. \tag{5}$$

In Eq. (5), h is Planck's constant c is the velocity of light $g''=1.98$, and $g'=2.44$, so that

$$\Delta\nu_\alpha(\mathrm{cm}^{-1})=9\times10^{-5}\Delta H. \tag{6}$$

The fractional change in light intensity is then given by

$$\Delta I=5.6\times10^{-9}(\Delta H/\delta)^2, \tag{7}$$

where ΔH is in gauss and δ in cm^{-1}. The width δ was determined by the slit width of the spectrometer and was approximately 0.2 cm^{-1}. For $\Delta H=200$ G the fractional change in light intensity thus becomes 0.56% and comparable with the change in light intensity due to the EPR signal.

However, since this background is coherent, it could be eliminated by taking one magnetic field sweep with the microwave power on and then the next with the microwave power off, and subtracting the two from each other. This subtraction was performed electronically by gating the analyzer into *add* and *subtract* modes on alternate sweeps. A block diagram of the system is shown in Fig. 4 and the appropriate timing sequence is given in Fig. 5. The sweep voltage supplied the triangular modulation for the field sweep coils and a syncronous pulse to start the analyzer sweep. The sweep time of the analyzer was made slightly less than the period of the sweep generator. After the analyzer, which was operated in a time mode, swept through its 400 channels it sent out an end-of-sweep pulse. This end-of-sweep pulse triggered a bistable multivibrator which turned the microwave power on and off on alternate cycles and also gated the analyzer into alternate *add* and *subtract* modes. The dead time between the change of klystron mode and the start of analyzer sweep eliminated the recording of troublesome switching transients. An illustrative light signal is drawn in Fig. 5 which shows both the unwanted background change in light intensity and a hypothetical 3-line EPR signal when the microwave power is on. The accumulated average signal in which the background has been subtracted is shown as a positive signal.

The 8-line hyperfine pattern in the $\bar{E}$ state of Al_2O_3:V^{2+}, obtained in the manner just outlined, is shown in Fig. 6. Only half a sweep cycle corresponding to a magnetic field sweep in one direction (200 channels) is shown. The nonlinearity of the magnetic field sweep is due to the distortion of the magnetic field sweep by the eddy current shielding of the microwave cavity.

The magnetic field sweep was calibrated by means of a proton NMR probe and the microwave frequency by a wavemeter calibrated to 1 part in 10^4. Eddy-current shielding by the microwave cavity of the magnetic field sweep reduced the size and phase shifted the sweep at the sample as compared to the NMR probe. For the most accurate measurements, the sweep field was centered about a given hyperfine line and reduced to ± 25 G to minimize this effect. In this way, an accuracy of 1 part in 2×10^3 was achieved in the determination of the position of the EPR lines.

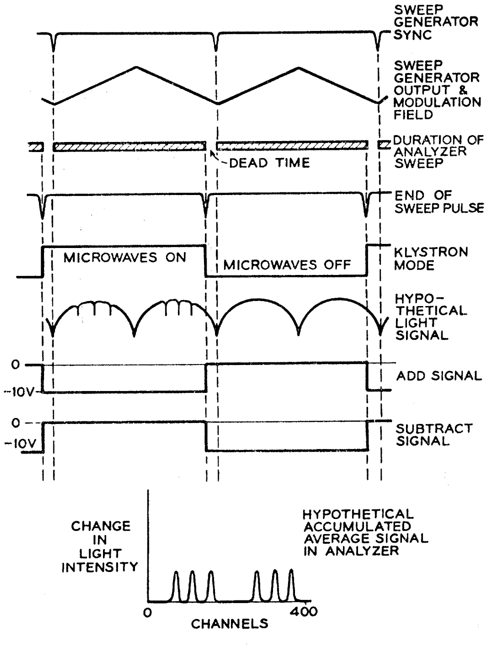

FIG. 5. Timing sequence of voltages for the experimental arrangement shown in Fig. 4. The sweep signal and syncronous pulse were supplied by the function generator. The syncronous pulse started the analyzer sweep whose period was slightly shorter than the triangular sweep period. At the end of the analyzer sweep an end-of-sweep pulse was emitted which triggered a bistable multivibrator. This performed two functions: It turned the microwave power on and off and gated the analyzer into *add* and *subtract* modes on alternate sweeps.

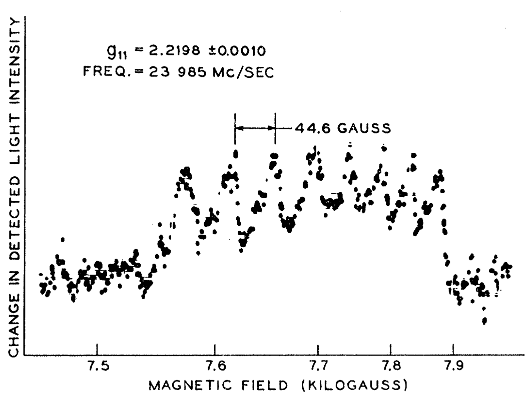

FIG. 6. Excited-state EPR signal in the $\bar{E}(^2E)$ state of V^{2+} in Al_2O_3. This shows the signal in one-half cycle of the triangular wave. The nonlinearity of the field sweep is due to the distortion of the magnetic field by eddy-current shielding of the microwave cavity.

3. *Use of Multichannel Analyzer for Relaxation Measurements*

The method used to measure the spin-lattice relaxation time in $\bar{E}$ of V^{2+} is essentially the same as that outlined in Sec. V of Ref. 2. The sample is continuously illuminated with mercury light to maintain an equilibrium population in the Zeeman levels of $\bar{E}$. The magnetic field is adjusted for resonance on one of the excited-state hyperfine transitions and the intensity of one of the fluorescent Zeeman optical components, for example, line α in Fig. 2, is monitored. When the microwave power is switched on, inducing transitions between corresponding m_I components of $\bar{E}$, the intensity of α decreases. When the microwave power is switched off, the intensity of line α recovers to its equilibrium value with a recovery time τ given by

$$1/\tau = 1/T_1 + 1/\tau_R. \qquad (8)$$

Here T_1 is the spin-lattice relaxation time and τ_R is the radiative lifetime. Equation (8) is derived in Ref. 2. This change in light signal was, of course, too weak to be seen on the oscilloscope so the method of continuous averaging using a multichannel analyzer as described in Ref. 2 was employed. The only variation from the procedure there described is to register the light signal as individual photons directly into the multichannel analyzer. This was feasible as the light signal for the V^{2+} was so weak[18] that "pileup" of counts was no problem. A syncronous pulse from the square-wave generator, used to modulate the klystron, would start the analyzer sweeping through typically 200 channels in a time corresponding to a single on-off cycle of the microwave modulation. In some cases runs as long as 2 to 3h were needed to obtain accurate relaxation data.

---

[18] In contrast, the light signal in ruby was so strong that pileup of light pulses was often encountered. It was therefore more feasible in the case of ruby to integrate the output of the phototube, and convert this integrated signal by means of analog to digital conversion into pulses that could then be counted by the analyzer as described in Ref. 2.

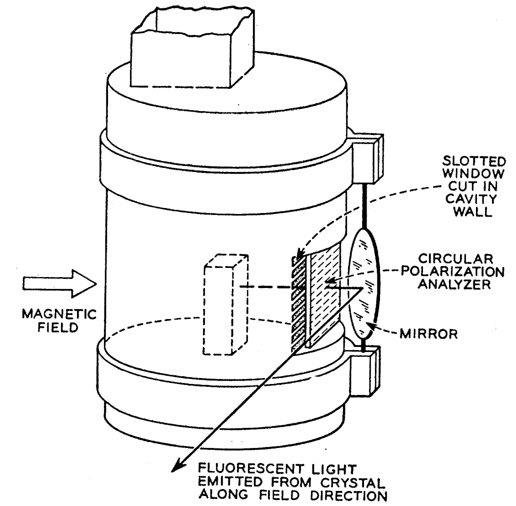

FIG. 7. Arrangement to detect circularly polarized light from the crystal of Al_2O_3:Mn^{4+} in the microwave cavity. The crystal was illuminated from below through a hole cut in the base of the cavity beneath the crystal. Horizontal slits cut in the cavity wall form a window to view the fluorescence. A circular-polarization analyzer, consisting of a $\lambda/4$ plate and linear polizer, was placed at the window and transmitted light only of the desired sense of circular polarization in the direction of the magnetic field. A small mirror deflected the transmitted light in the conventional direction perpendicular to the magnetic field.

The number of on-off cycles averaged in this time could be as large as 10^6 and implied a signal-to-noise improvement of 10^3 over that for a single pass. The digital data stored in each memory channel corresponding to the total number of light pulses registered in each channel were presented as an analog signal on the analyzer cathode-ray-tube (CRT) display as is sketched in Fig. 3. The second half-cycle of the display represents the return to equilibrium of the $\bar{E}$ population. The data were punched out on paper tape and converted to punch cards which were then processed by an IBM 7090 to yield a semi-log plot of light signal versus time as well as a least-squares fit of τ.

D. Mn^{4+} in Al_2O_3

1. Scheme to Detect Circularly Polarized Light

To observe circularly polarized fluorescence one must detect radiation emitted by the ions in a direction parallel to the magnetic field. This necessitates either observing the radiation through a hole drilled in the magnet pole face or deflecting the light once it leaves the crystal so that it leaves the magnet gap in the more conventional direction perpendicular to the magnetic field. The second method allowed a more efficient gathering of light flux and was chosen. Subsidiary experiments to determine to what extent the circular-polarization selection rules of Fig. 2 are obeyed were carried out on ruby. By reducing depolarization as much as possible it was found that the selection rules are obeyed to approximately 90%. To reduce depolarization a black matt copper oxide coating was put on the inside of the cavity and this absorbed all fluorescence except that which was transmitted directly through the window. The circular-polarization analyzer, consisting of a $\lambda/4$ plate and linear polarizer, was placed at the window of the cavity so that of the light emitted by the crystal and leaving the window, only the correct circular polarization was viewed. Any depolarization of light in the liquid helium or liquid nitrogen, or at the walls of the Dewar, was now of no consequence. A small mirror, just outside the cavity window, deflected the analyzed light through 90° towards the photomultiplier. This arrangement is shown in Fig. 7.

2. Estimate of Signal Size

Most of the experiments on Mn^{4+} were carried out at a microwave frequency of 48 kMc/sec. At 2°K, the intensity of right circularly polarized light is approximately 10% less than when both Zeeman levels are equally populated. Mn^{55} ($\sim$100% abundant) has a nuclear spin of $\frac{5}{2}$ and consequently we expect a 6-line hyperfine pattern. When resonance occurs at one of these lines one hopes at best for a 2% change in the intensity of right circularly polarized light. Since the fluorescence was focused directly onto the photomultiplier without having to pass through the spectrometer, the light flux impinging upon the photomultiplier was high. Coupled with the greater quantum efficiency of phototubes at 6900 Å (position of R_1 line in Mn^{4+}) compared to 8600 Å (position of R_1 line in V^{2+}) this resulted typically in a *detected* flux of 3×10^7 photons/sec. Thus, with a 1-sec integration time, shot noise in the light beam was approximately 0.02% compared to the

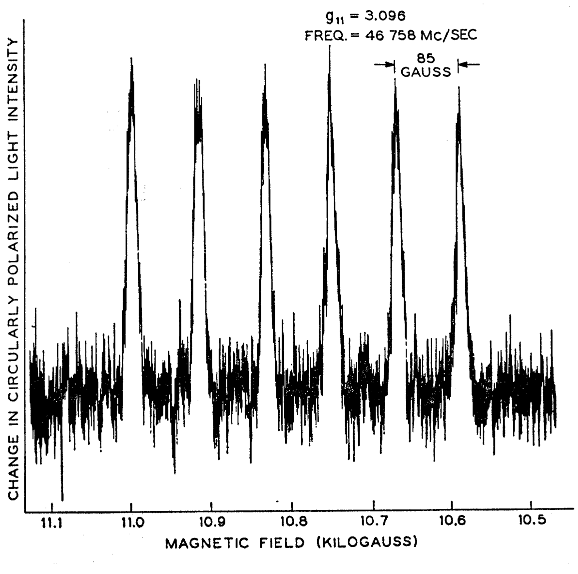

FIG. 8. Excited-state EPR signal in the $\bar{E}(^2E)$ state of Mn^{4+} in Al_2O_3. This shows the change in right circularly polarized light as the magnetic field swept through resonance with microwave power applied.

anticipated signal of 2% so that a $S/N\sim 100$ was expected. Actually, the S/N was observed to be less by close to an order of magnitude. Once again this reduction in signal over that anticipated for complete saturation of the microwave line was most likely due to "hole burning" in the microwave line due to the weakness of spin diffusion because of the small value of $g_\perp$.

3. *Observation of EPR*

Because of the large signal-to-noise ratio expected for Mn^{4+}, lock-in detection techniques could be used. The experimental arrangement of Fig. 2 using lock-in detection was employed. The magnetic field was varied slowly through resonance. The microwave power was chopped at 300 cps and the resultant 300-cps component in the circularly polarized light output was detected by the lock-in detector and fed to a pen recorder. A recorder trace taken with a 3-sec integration time is shown in Fig. 8. No effort was made to stabilize either the microwave source or the pumping light. It is estimated that these signals were obtained from approximately 5×10^{10} spins in the excited state.

The cavity frequency was measured by comparison with a multiple of the output of a calibrated X-band stabilized oscillator. The magnetic field was calibrated by means of a proton NMR probe.

4. *Measurements of Relaxation Times*

Use was made of the multichannel analyzer to measure the recovery of the light signal after switching off the microwaves. The arrangement is exactly the same as was used for V^{2+} (Sec. III C) except that the change in intensity of circularly polarized light was used to monitor resonance in this case. Relaxation data were obtained over the temperature range 2 to 9°K.

IV. HYPERFINE STRUCTURE IN THE $\bar{E}(^2E)$ STATE

The spin Hamiltonian for the $\bar{E}(^2E)$ state of a $(3d)^3$ ion in Al_2O_3 in the presence of a magnetic field is given by

$$\mathcal{H}=g_{\parallel}\beta H_zS_z'+g_\perp\beta(H_xS_x'+H_yS_y')+A_{\parallel}'I_zS_z'+A_\perp'(I_xS_x'+I_yS_y')-g_I\beta_NH_zI_z. \tag{9}$$

Here S' is the fictitious spin of $\frac{1}{2}$ which is opposite in sign to the real spin of $\frac{1}{2}$ as explained in Appendix A.

The z direction is taken along the c axis, g_I is the nuclear g value, and β_N is the nuclear Bohr magneton. The g values for V^{2+} measured by Sturge[14] from optical data are $|g_{\parallel}|=2.22$ and $g_\perp\approx 0.05$. For Mn^{4+} Crozier[16] finds $|g_{\parallel}|=3.08$ and $g_\perp<0.3$. Our more accurate microwave measurements of $g_{\parallel}$ for these ions as determined in this work are listed in Table II along with those measured earlier for Cr^{3+}.[1] The near zero value of $g_\perp$ for these ions in the $^2\bar{E}$ state prevented a determination of $A_\perp$. With the magnetic field directed along the c axis, the usual selection rules $\Delta m_s=\pm 1$ and $\Delta m_I=0$ result in microwave absorptions at a frequency ν given by

$$h\nu=g_{\parallel}\beta H_0+A_{\parallel}'m_I \tag{10}$$

with $(2m_I+1)$ hyperfine components as indicated in Figs. 6 and 8 for V^{2+} and Mn^{4+}, respectively.

The experimentally determined hyperfine interactions for these d^3 ions in $\bar{E}$ are listed in Table II and are also expressed in terms of the hyperfine field per *unit* unpaired real electron spin ($S=1$) given by

$$H_{\mathrm{hf}}=-A_{\parallel}'/g_I\beta_N=+A_{\parallel}/g_I\beta_N. \tag{11}$$

The choice of signs for $g_{\parallel}$ and $A_{\parallel}'$ are explained in the Appendix, but there should be no ambiguity in interpreting the sign of H_{hf}; by convention a *positive* hyperfine field is one which points *opposite* to the *real* electron spin.

To compare the observed value of A' with the theoretically expected value, we consider the hyperfine interaction expressed in terms of its component parts[19]:

$$\mathcal{H}=P\left(\sum_k \mathbf{l}_k\cdot\mathbf{I}-\kappa\mathbf{S}\cdot\mathbf{I}+\tfrac{1}{7}\sum_k \mathbf{a}_k\cdot\mathbf{I}\right), \tag{12}$$

where

$$P=2g_I\beta\beta_N\langle 1/r^3\rangle, \tag{13}$$

and

$$\mathbf{a}_k=4\mathbf{s}_k-(\mathbf{l}_k\cdot\mathbf{s}_k)\mathbf{l}_k-\mathbf{l}_k(\mathbf{l}_k\cdot\mathbf{s}_k). \tag{14}$$

The three terms on the right in Eq. (12) are respectively the orbital, core-polarization, and dipolar hyperfine interactions ($H_{\mathrm{hf}}{}^{\mathrm{orb}}$, $H_{\mathrm{hf}}{}^{\mathrm{cp}}$, $H_{\mathrm{hf}}{}^{\mathrm{dip}}$). $\sum_k$ is the summation over all the d electrons. Note that the writing of the core-polarization hyperfine field (cphf) in this way is not too meaningful as there is no reason to believe that it is simply related in any way to $\langle 1/r^3\rangle$. We therefore choose not to speak in terms of κ and rewrite Eq. (12) as

$$\mathcal{H}=P\sum_k\left(\mathbf{l}_k\cdot\mathbf{I}+\tfrac{1}{7}\mathbf{a}_k\cdot\mathbf{I}\right)+A_{\mathrm{cp}}\mathbf{I}\cdot\mathbf{S}=A'\mathbf{I}\cdot\mathbf{S}'. \tag{15}$$

If the orbital angular momentum were totally quenched, then we would only have the cphf. As the g shift measures the unquenched orbital angular momentum, there is a direct relationship between the orbital hf field per unit electron spin and g shift given first by Abragam and Pryce[20] as

$$H_{\mathrm{hf}}{}^{\mathrm{orb}}=2\beta\langle 1/r^3\rangle\Delta g_L \tag{16}$$

$$=+125\langle 1/r^3\rangle_{\text{atomic units}}\Delta g_L kG, \tag{17}$$

where Δg_L is the orbital g shift. In the $^4A_2$ ground state of V^{2+}, Cr^{3+}, and Mn^{4+}, the g shifts are exceedingly small so that the major hf field is that due to core polarization. Taking account of the very small orbital

---

[19] J. S. Griffith, *The Theory of Transition Metal Ions* (Cambridge University Press, New York, 1961).

[20] A. Abragam and M. H. L. Pryce, Proc. Roy. Soc. (London) **A205**, 135 (1951).

TABLE II. Experimentally determined values of the hyperfine constants, and values of the other quantities considered in the discussion on hfs. The symbols are defined in the text.

Ion	$g_{\parallel}$[a]	$g_{\perp}$	$\Delta g_{\parallel}$	$\langle 1/r^3\rangle_{\text{a.u.}}$[b]	$H_{\text{hf}}^{\text{orb}}$ (kG)	$H_{\text{hf}}^{\text{cp}}$ (kG)	$H_{\text{hf}}^{\text{dip}}$ (kG)	$H_{\text{hf}}^{\text{total}}$ (kG)	$A'_{\parallel}{}^{\text{theor}}$[c] ($10^{-4}$ cm^{-1})	$A'_{\parallel}{}^{\text{exp}}$[d] ($10^{-4}$ cm^{-1})
V^{2+}[e]	$(-)2.2198\pm0.001$	≈ 0.05	0.218	2.747	$+74.8$	-193	-10.7	-128	$+48.0$	$(+)46.3\pm1.5$
Cr^{3+}[f]	$(-)2.445\pm0.001$	≈ 0.06	0.443	3.958	$+219$	-193	-31	-5.0	$+0.4$	<2
Mn^{4+}[e]	$(-)3.0959\pm0.0006$	≤ 0.3	1.093	5.4	$+740$	-193	-88	$+459$	-161	$(-)123\pm3$

[a] See Appendix A for discussion of the sign of $g_{\parallel}$ and $A_{\parallel}'$.

[b] R. E. Watson, Solid State and Molecular Theory Group, Massachusetts Institute of Technology, Technical Report No. 12, 1959 (unpublished).

[c] To compare these values of $A_{\parallel}'$ with ground-state $A_{\parallel}$ values, the sign of $A_{\parallel}'$ must be reversed in order for it to correspond to a real electron spin S.

[d] In these experiments the sign of the hf splitting parameter is not measured, but on the basis of the theoretical analysis, the sign is believed to be that indicated in the parenthesis.

[e] Present work.

[f] See Ref. 2.

hf field in the $^4A_2$ states as given by Eq. (18), and using the ground-state experimental data,[15,21–23] one finds that the cphf per unit spin is $H_{\text{hf}}^{\text{cp}} = -193\,000$ kG, i.e., it is essentially the same for all the three ions.[5] Since the electron distribution in the ^2E state is the same as in the $^4A_2$ ground state (both are t_2^3 states), we assume that the cphf field in the ^2E state is the same as in the ground state.

The orbital hf fields in $\bar{E}$ are calculated from the g shifts using Eq. (17) and the $\langle 1/r^3\rangle$ values given by Freeman and Watson,[24] and are listed in column six of Table II. Note how large the orbital hf field of Mn^{4+} is, and that it is the dominant contribution to the total hyperfine field.

No simple relationship such as Eq. (16) exists which relates $H_{\text{hf}}^{\text{dip}}$ to some other easily observed quantity as a g shift. To calculate $H_{\text{hf}}^{\text{dip}}$ one must have knowledge of the wave function of the excited states. However, we may circumvent this task because of a fortuitously favorable approximation that can be made for the t_2^3 configuration. Let us represent the ^2E state by $|^2E\rangle' = |^2E\rangle + \alpha|^2T_2\rangle + \beta|^2T_1\rangle$, where α and β are admixture coefficients of these other doublets due to spin-orbit coupling and trigonal field. Sugano and Tanabe[9] have shown that the major contribution to the g shift comes from matrix elements of $\sum_k l_k^z$ only between $|^2E\rangle$ and $|^2T_1\rangle$ of the type

$$\langle {}^2E, u_+ - \tfrac{1}{2} | \sum_k l_k^z | {}^2T_1 a_+ - \tfrac{1}{2}\rangle. \tag{18}$$

One can easily show by using the wave functions given in Appendix B along with the one-electron matrix elements of a^z also given there, that

$$\langle {}^2E, u_+ - \tfrac{1}{2} | \sum_k l_k^z | {}^2T_1 a_+ - \tfrac{1}{2}\rangle = -\langle {}^2E, u_+ - \tfrac{1}{2} | \sum_k a_k^z | {}^2T_1 a_+ - \tfrac{1}{2}\rangle. \tag{19}$$

While there are additional matrix elements of a^z of the type $\langle {}^2E, u_+ - \frac{1}{2} | a^z | {}^2T_1 a_0 + \frac{1}{2}\rangle$ which vanish for l^z, the coefficient of admixture of $|{}^2T_1, a_0 + \frac{1}{2}\rangle$ is much smaller than that of $|{}^2T_1, a_+ - \frac{1}{2}\rangle$ and so it may be neglected. To the extent of this approximation involving the equivalence within a sign of appropriate matrix elements of l^z and a^z, we may write for $\bar{E}(^2E)$

$$H_{\text{hf}}^{\text{dip}} \simeq -\tfrac{1}{7} H_{\text{hf}}^{\text{orb}}. \tag{20}$$

The values of $H_{\text{hf}}^{\text{dip}}$ obtained from this expression are entered in Table II for V^{2+} and Cr^{3+}. This approximation is probably best in the limit of strong cubic crystal field (the case of Mn4+) and poorest in the case of weak crystal field (V^{2+}) where there is greater configuration mixing and the representation of the doublet states as t_2^3 breaks down. However, the actual size of $H_{\text{hf}}^{\text{orb}}$ is smallest in the case of V^{2+} so that one makes a small and probably negligible *absolute* error in this case. In the case of Mn^{4+}, using the wave function given in Appendix B, one finds that matrix elements of the type $\langle {}^2E, u_+ - \frac{1}{2} | a^z | {}^2T_1 a_0 + \frac{1}{2}\rangle$ subtract approximately 15% from the dipolar field above that given by Eq. (20) and because of the large absolute value of $H_{\text{hf}}^{\text{dip}}$ this is included in $H_{\text{hf}}^{\text{dip}}$ for Mn^{4+} in Table II.

Referring to Table II, one sees that there is quite good agreement between the calculated total hf field and that observed experimentally. The failure to obtain a better agreement in the case of Mn^{4+} could be due to the fact that because of the large value of $H_{\text{hf}}^{\text{dip}}$, the approximation of staying within the t_2^3 representation leads to the largest errors for this ion. However, even more simply, it could be due to the inaccuracy of $\langle 1/r^3\rangle$. In view of the large value of the orbital hyperfine field in the case of Mn^{4+}, an error in the value of $\langle 1/r^3\rangle$ is more serious for this ion than for V^{2+} or Cr^{3+}. Note that a decrease of about 14% in $\langle 1/r^3\rangle$ would

---

[21] A. A. Manenkov and A. M. Prokhorov, Zh. Eksperim. i Teor. Fiz. **31**, 346 (1956) [English transl.: Soviet Phys.—JETP **4**, 288 (1957)].

[22] G. M. Zverev and A. M. Prokhorov, Zh. Eksperim. i Teor. Fiz. **34**, 513 (1958) [English transl.: Soviet Phys.—JETP **7**, 354 (1958)].

[23] J. Lambe and C. Kikuchi, Phys. Rev. **118**, 71 (1960).

[24] A. Freeman and R. E. Watson, in *Treatise on Magnetism*, edited by G. Rado and H. Suhl (Academic Press Inc., New York, 1965), Vol. 11A; also R. E. Watson, Solid State and Molecular Theory Group, Massachusetts Institute of Technology, Technical Report No. 12, 1959 (unpublished).

reduce $H_{\mathrm{hf}}^{\mathrm{orb}}$ sufficiently to bring experimental and theoretical values into precise agreement. Such a decrease in $\langle 1/r^3 \rangle$ from the free-ion value is not at all unreasonable for Mn^{4+} in $\mathrm{Al_2O_3}$, since it is the most covalent of the isoelectronic ions being studied here. In addition, there is an assumption that is implicit in Eq. (16) with regard to the orbital hyperfine operator that $\sum_i \langle l_i/r_i^3 \rangle = \sum_i \langle l_i \rangle \langle 1/r_i^3 \rangle$. This is true as long as $\langle 1/r_i^3 \rangle$ is the same for all the orbitals involved which would be the case as long as we stay within a d^n configuration and retain the ionic approximation. However, if for the very covalent Mn^{4+} we more properly consider a molecular orbital involving ligand p orbitals, for example, this is no longer true. If then the unpaired spins in the ligand orbitals should contribute more strongly to the orbital magnetism of the complex (and hence g shift) than to $H_{\mathrm{hf}}^{\mathrm{orb}}$, Eq. (16) would tend to overestimate $H_{\mathrm{hf}}^{\mathrm{orb}}$. It is not entirely clear, however, in which direction this latter effect would operate.

V. SPIN-LATTICE RELAXATION

As described in Sec. III, when the microwave saturating power is turned off, with the external magnetic field set for resonance in the excited state, the monitored fluorescent light intensity returns to equilibrium at an exponential rate with a time constant τ. τ is given by[2]

$$1/\tau = 1/\tau_R + 1/T_1, \qquad (21)$$

where τ_R is the radiative decay time of the R lines. The rate equations leading to Eq. (21) are examined in detail in Ref. 2. As τ_R is known from other independent measurements, a measurement of τ yields T_1. No radiative trapping occurs in the R lines of V^{2+} and Mn^{4+}, so that all Zeeman components of R_1 have identical fluorescence decay times. For V^{2+}, τ_R is independent of temperature between 1.5 and 2.2°K (the region studied) and its value is 65 msec.[14] Similarly, for Mn^{4+}, τ_R is independent of temperature between 2 and 10°K (the region studied) and its value is 0 83 msec.[15]

The radiative lifetime usually sets a limit on the longest T_1 that can be measured as it is very difficult to extract an accurate value of T_1 from τ when $T_1 > 10\tau_R$.

The subject of spin-lattice relaxation has been treated in detail in a number of places.[25–28] It is customary to divide spin-lattice relaxation into three processes, i.e., the direct, Orbach, and Raman. In a more general way the Orbach process may be viewed as a special case of the direct processes in a multilevel system.[29] The possibility of observing a direct process between the Zeeman components of $\bar{E}(^2E)$ has been examined in Ref. 21. It was there shown that, for $H_0 \parallel$ to the c axis, it will be of the order of seconds in our temperature range so that it will be masked by the radiative lifetime.

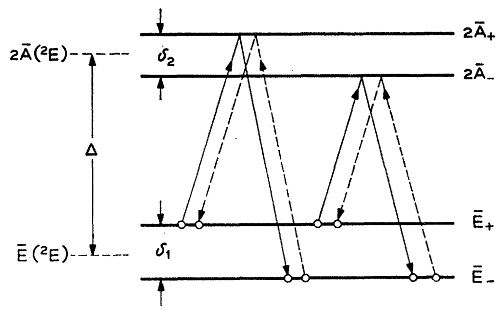

FIG. 9. Transitions involved in the Orbach relaxation process. An ion in, say, the $\bar{E}_+$ level absorbs a phonon of approximate energy Δ and rises to one of the two $2\bar{A}$ levels from which it decays by phonon emission to the $\bar{E}_-$ level. The reverse path from $\bar{E}_-$ to $\bar{E}_+$ exists and is shown by the dashed transitions. Each of these two-step processes involves both a spin-flip and a non-spin-flip transition.

The spin-lattice relaxation in the temperature region covered in our experiments is dominated by the Orbach process as was demonstrated in ruby.[2] The weakness of the Raman process as compared to the Orbach process in corundum is due to the hardness of these crystals. The Raman relaxation rate varies as $1/v^{10}$ whereas the Orbach relaxation rate goes as $1/v^5$, where v is the velocity of sound. In $\mathrm{Al_2O_3}$, v is quite large and equal to $\sim 10^6$ cm/sec,[30] so that one anticipates a very weak Raman process. This is borne out by studies of the spin-lattice relaxation in the ground state of Co^{2+} in $\mathrm{Al_2O_3}$, where a direct and Orbach process are seen but no Raman process is observed even up to 25°K.[31–33] This situation is to be contrasted with that in the much softer water crystals, such as the double nitrates and ethyl sulfates, for which $v \sim 2\times 10^5$ cm/sec so that Raman processes are seen as low as the He temperature range.[28]

The transitions involved in the Orbach process are represented in Fig. 9. An ion in, say, the $\bar{E}_+$ level absorbs a phonon of energy $\approx\Delta$ and rises to one of the $2\bar{A}$ levels from which it decays by spontaneous phonon emission to $\bar{E}_-$. One of these steps involves an $\bar{E} \leftrightarrow 2\bar{A}$ transition in which the spin is unchanged and the other involves a similar transition in which the spin is flipped. A theoretical investigation[34] of these transition rates

---

[25] J. H. Van Vleck, Phys. Rev. **57**, 426 (1940).

[26] R. Orbach, Proc. Roy. Soc. (London) **A264**, 458 (1961).

[27] R. D. Mattuck and M. W. P. Strandberg, Phys. Rev. **119**, 1204 (1960).

[28] P. L. Scott and C. D. Jeffries, Phys. Rev. **127**, 32 (1962).

[29] A. A. Manenkov and A. M. Prokhorov, Zh. Eksperim. i Teor. Fiz. **42**, 1371 (1962) [English transl.: Soviet Phys.—JETP **15**, 951 (1962)].

[30] As can be seen from the values of the elastic constants given by H. B. Huntington, in *Solid State Physics*, edited by F. Seitz and D. Turnbull (Academic Press Inc., New York, 1956), Vol. VII.

[31] G. M. Zverev and A. M. Prokhorov, Zh. Eksperim. i Teor. Fiz. **39**, 57 (1960) [English transl.: Soviet Phys.—JETP **12**, 41 (1961)].

[32] J. Geusic, Solid State Maser Research, Third Quarterly Report, 1961, Part V, p. 28 (unpublished). U. S. Army Signal Supply Agency Contract No. DA 36-039 SC 85357.

[33] G. M. Zverev and A. M. Prokhorov, Zh. Eksperim. i Teor. Fiz. **42**, 1186 (1962) [English transl.: Soviet Phys.—JETP **15**, 820 (1962)].

[34] M. Blume, R. Orbach, A. Kiel, and S. Geschwind, Phys. Rev. **139**, A314 (1965).

shows that the spin-flip process is the slower and is the "bottleneck" which determines the Orbach relaxation time.

{*Note added in proof.* A recent photon echo experiment [N. A. Kurnit, I. D. Abella, and S. R. Hartmann, *Physics of Quantum Electronics* (McGraw-Hill Book Company, Inc., New York, 1966), p. 267] in conjunction with the relaxation data of Ref. 2 indicates that the spin-flip time $T_{2\bar{A}_+\rightarrow\bar{E}_-}$ is only approximately one-fourth the value of the non-spin-flip time $T_{2\bar{A}_+\rightarrow\bar{E}_+}$ calculated in Ref. 34. The origin of this discrepancy is as yet unresolved.}

It was shown in Ref. 2 that the Orbach relaxation time is given by

$$T_1=\tfrac{1}{4}T_{2\bar{A}_+\rightarrow\bar{E}_-}\exp(\Delta/kT)[\cosh(\delta_1/2kT)\times\cosh(\delta_2/2kT)]^{-1}, \quad (22)$$

where $T_{2\bar{A}_+\rightarrow\bar{E}_-}$ is the time for spontaneous decay by phonon emission from $2\bar{A}$ to $\bar{E}$ in which the spin is flipped.[34] The term containing δ_1 and δ_2 is a correction which makes allowance for the effect of the Zeeman splittings of the $\bar{E}$ and $2\bar{A}$ levels on the Bose exponential factor and is only important at the lowest temperatures where $\delta\sim 2kT$.

We briefly review the theoretical treatment of direct process relaxation $T_{2\bar{A}\rightarrow\bar{E}}$ as given in Ref. 34. The orbit-lattice interaction, i.e., the energy of the ion in the crystal field, is written as a power series in the strain ϵ:

$$\mathcal{H}_{O-L}=V_0+V^{(1)}\epsilon+V^{(2)}\epsilon^2+\cdots. \quad (23)$$

This interaction can be used to describe perturbations introduced both by laboratory produced static strains as well as by dynamic strains induced by phonons. The probability of a direct transition from $2\bar{A}$ to $\bar{E}$ by the dynamic strain perturbation is

$$1/T_{2\bar{A}\rightarrow\bar{E}}=w_{2\bar{A}\rightarrow\bar{E}}$$
$$=2\pi/\hbar\,|\langle\bar{E}|V^{(1)}|2\bar{A}\rangle|^2|\langle\bar{n}+1|\epsilon|\bar{n}\rangle|^2\rho_\Delta, \quad (24)$$

where $\bar{n}$ is the average occupation number of phonons of energy Δ and ρ_Δ is the density of phonon states of energy Δ. The frequency and temperature dependence of w is contained in the last two terms of Eq. (24). In the past, the matrix elements of $V^{(1)}$ were estimated by adopting a point-charge model, but this yields at best only order of magnitude results. It is now more customary to make use of the fact that the matrix elements of $V^{(1)}$ in Eq. (24) are related to those appearing in the shift of these levels with static strain.[35,36]

Actually, $V^{(1)}\epsilon$ is a tensor dot product

$$\tilde{V}:\tilde{\epsilon}=\sum_{\Gamma,\gamma}V(\Gamma)c(\Gamma,\gamma)\epsilon(\Gamma,\gamma), \quad (25)$$

where Γ refers to an irreducible representation of the point group at the impurity ion site; γ is one of the basis vectors of Γ; $c(\Gamma,\gamma)$ are combinations of the spherical harmonics appropriate to the point symmetry, and $\epsilon(\Gamma,\gamma)$ are combinations of the strains which transform as $c(\Gamma,\gamma)$. Thus in general, in order to obtain the appropriate matrix elements of V needed in Eq. (24) from static-strain measurements a number of static-strain parameters would be needed; for example, for a general ${}^2E$ or Γ_8 quartet in C_3 symmetry, five strain parameters are needed.[37] However, it was shown in Ref. 34 that, by a fortunate set of circumstances peculiar to the ${}^2E$ level of d^3 ions, only strains of symmetry T_2, i.e., $\epsilon(T_2,\pm1)$, are important in the relaxation. The appropriate $V(T_2)$ may in turn be evaluated by using the Wigner-Eckart theorem from the single measurement of the change ΔE in the $2\bar{A}$-$\bar{E}$ separation with a static strain $\epsilon(T_2,0)$, i.e., a strain along the c axis. Thus the appropriate matrix element of $V^{(1)}$ in Eq. (24) can be evaluated by a single subsidiary static-strain measurement $\Delta E/T_{z'z'}$, where $T_{z'z'}$ is a static stress along the c axis. The procedure is expected to be valid as long as the phonons in question are of sufficiently long wavelength so that they produce a macroscopic strain. Note, however, that no assumption is being made about the local strain being the same as the macroscopic strain. From Ref. 34 the relaxation rate can be written as

$$w_{2\bar{A}_+\rightarrow\bar{E}_-}=1/T_{2\bar{A}_+\rightarrow\bar{E}_-}=\frac{27}{4}\left[\frac{\Delta E}{T_{z'z'}(S_{33}-S_{13})}\right]^2\times\frac{\Delta^3}{135\pi\rho\hbar^4}\left(\frac{1}{v_l^5}+\frac{3}{2v_t^5}\right)(\bar{n}+1). \quad (26)$$

In Eq. (26) S_{33} and S_{13} are the elastic compliance constants given by Huntington for Al_2O_3,[30] so that the expression in square brackets is the change in the $2\bar{A}$-$\bar{E}$ separation with static strain along the c axis.

In the isoelectronic sequence V^{2+}, Cr^{3+}, and Mn^{4+}, Δ is equal to 12, 29, and 80 cm^{-1}, respectively. Thus, by measuring $T_{2\bar{A}\rightarrow\bar{E}}$ in the Orbach process in the same crystal, we can verify the Δ^3 dependence of the direct-process rate for *non*-time-reversed states in the region $\Delta\gg kT$. For $\Delta\ll kT$ this rate would vary as Δ^2T. However, for such a check to be most meaningful it must also include a static-strain measurement of the orbit-lattice parameter $V^{(1)}$ which will vary from ion to ion in the same crystal. Indications of the validity of the Δ^3 dependence of the Orbach spin-lattice relaxation rate for Fe^{3+} in andalusite[38] and for Ce^{3+} in the ethyl sulfates[39] have recently been reported but in neither case is the matrix element of the orbit-lattice interaction connecting the states in question (separated by Δ) known, or its variation with Δ.

In accordance with Eq. (22),

$$T_1\cosh\delta_1/2kT\cosh\delta_2/2kT,$$

which we shall call T_1', should vary as $e^{\Delta/kT}$. This is the

---

[35] A. L. Schawlow, A. H. Piksis, and S. Sugano, Phys. Rev. **122**, 1469 (1961).

[36] M. D. Sturge, Phys. Rev. **131**, 1456 (1963).

[37] P. L. Donoho, Phys. Rev. **133**, A1080 (1964).

[38] I. I. Eru, S. A. Peskovatskii, and A. N. Chernets, Fiz. Tverd. Tela **7**, 363 (1965) [English transl.: Soviet Phys.—Solid State **7**, 293 (1965)].

[39] G. H. Larson, Phys. Rev. **150**, A264 (1966).

experimental quantity which is plotted versus $1/T$. Actually the difference between T_1 and T_1' is only of importance in our data in V^{2+} at the very lowest temperature.

Figure 10 shows an experimental plot of T_1' versus inverse temperature. If T_1' is fitted to $ce^{\Delta/kT}$, one finds $\Delta = 12.1 \pm 1.2$ cm^{-1} as compared with the experimental spectroscopic determination of $\Delta = 12.3$ cm^{-1}.[14] The constant c is found to be $c = 5.2 \times 10^{-8}$ sec. Most measurements were made at 24 kMc/sec (circles) but data were also taken at 48 kMc/sec (crosses). The results at the two frequencies are seen to coincide, further confirming the Orbach process. The longest T_1 measured was limited by the lowest temperature we could reach, which in turn was limited by the lowest-intensity exciting light that could be used and the pumping speed on the He bath, to 1.5°K. The shortest T_1 was governed by the resolving time of our multi-channel analyzer which was approximately 100 μsec.

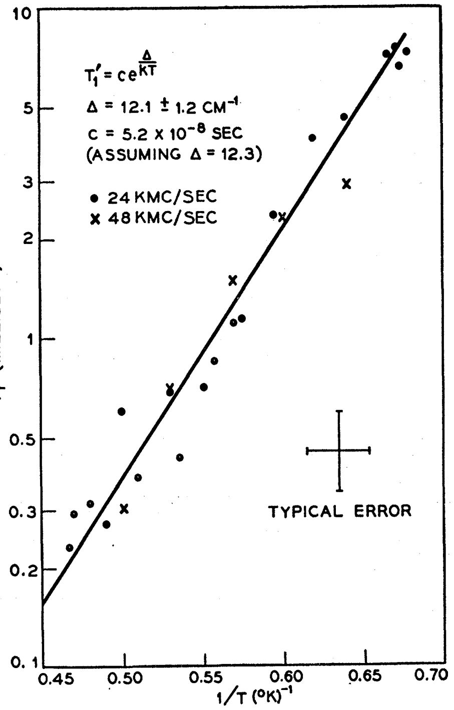

FIG. 10. Semilog plot of T_1' versus $1/T$ in the $\bar{E}(^2E)$ state of V^{2+} in Al_2O_3. The heavy line is a best fit to a $T_1' = ce^{\Delta/kT}$ function and gives $\Delta = 12.1 \pm 1.2$ cm^{-1}, very close to the optically measured value of 12.3 cm^{-1}. The value of c determined from the data is 5.2×10^{-8} sec.

Figure 11 shows the temperature variation of the recovery time τ of the Mn^{4+} light signal after turning off the microwaves. The arrow on the ordinate corresponds to the radiative lifetime $\tau_R = 0.83$ msec. It is seen that up to about 6°K, $T_1 \gg \tau_R$, so that τ is dominated by τ_R. It is therefore possible to extract meaningful values of T_1 from τ by using Eq. (21) only for values of T above 6°K. The range of T_1 that could be covered in this case as compared to V^{2+} was therefore limited on the high side by the shorter τ_R and on the low side again by the time resolution of our apparatus. A plot of T_1' over this limited temperature range, shown as a semilog plot of T_1' versus $1/T$, is seen in Fig. 12. The heavy line is the best fit to a $T_1' = ce^{\Delta/kT}$ curve and gives $\Delta = 72 \pm 20$ cm^{-1}, which is close to the optically observed 80-cm^{-1} splitting, and $c = 1.6 \times 10^{-10}$ sec.

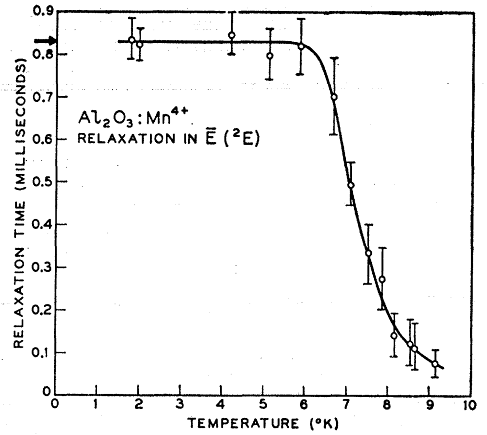

FIG. 11. Observed recovery time τ of the manganese fluorescence after turning off the microwave power plotted as a function of temperature. The arrow on the ordinate corresponds to the radiative lifetime $\tau_R = 0.83$ msec. Up to about 6°K τ is dominated by τ_R.

Because of the limited accuracy of our data relative to the very narrow range of T_1 that could be measured, one can also obtain a reasonably good fit to the data with $T_1 \sim T^n$. In the case of V^{2+}, $n \sim +9.5 \pm 0.5$ and for

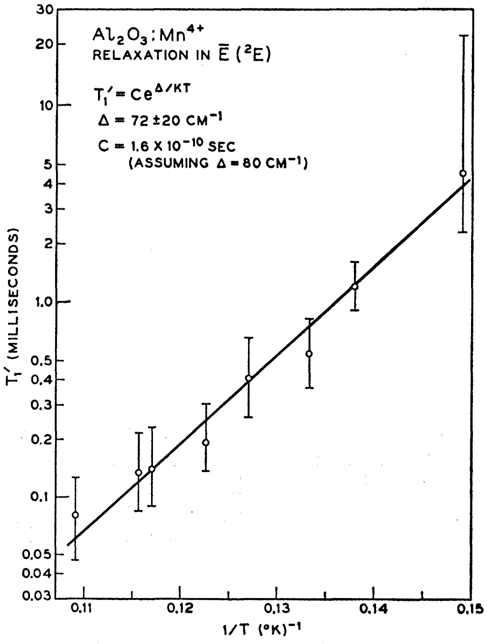

FIG. 12. Semilog plot of T_1' versus $1/T$ for the $\bar{E}(^2E)$ state of Mn^{4+} in Al_2O_3. The heavy line is a best fit to a $T_1' = ce^{\Delta/kT}$ curve and gives $\Delta = 72 \pm 20$ cm^{-1}. From the data we obtain $c = 1.6 \times 10^{-10}$ sec.

TABLE III. The experimentally measured values of the direct-process relaxation time $T_{2\bar{A}_+\to\bar{E}}$ are compared with theoretical values for the three ions in Al_2O_3. The experimental values of the ^2E crystal-field splitting Δ are given for each ion as well as the strain parameters $\Delta E/T_{z'z'}$ and $\Delta E/T_{z'z'}\,(S_{33}-S_{13})$. These strain parameters are defined in the text.

Ion	Δ (cm^{-1})	$T_{2\bar{A}_+\to\bar{E}_-}{}^{\text{theor}}$ (sec)	$T_{2\bar{A}_+\to\bar{E}_-}{}^{\text{expt}}$ (sec)	$\Delta E/T_{z'z'}$ in units of cm^{-1} per 100 kg/mm^2	$\Delta E/[T_{z'z'}(S_{33}-S_{13}]$ in units of cm^{-1}/per unit strain ϵ_0
V^{2+}	12.3	1.7×10^{-7}	2.1×10^{-7}	-0.90	3.9×10^2
Cr^{3+}	29	3.0×10^{-8}	1.5×10^{-8}	-0.57	2.46×10^2
Mn^{4+}	80	2×10^{-9}	6.4×10^{-10}	$+0.50$	-2.16×10^2

Mn^{4+} $n\sim+13.7\pm0.5$. This value of n for Mn^{4+} is far from any known Raman process. For V^{2+} n is embarrassingly close to 9, the usual value for a Raman process in a Kramers salt. However, the fact that an equally good fit to an exponential gives a value of Δ that coincides with the spectroscopic value well within the experimental error for V^{2+}, Cr^{3+}, and Mn^{4+}, coupled with the reasons given above for not anticipating any Raman process until much higher temperatures, makes it appear certain that the relaxation data is correctly being interpreted in terms of an Orbach process. This confidence is further justified by an examination of the values $T_{2\bar{A}\to\bar{E}}$ which we now proceed to discuss.

The experimental value $T_{2\bar{A}-\bar{E}}$ appearing as the coefficient $\frac{1}{4}T_{2\bar{A}\to\bar{E}}$ in front of the exponential in the Orbach process is given in Table III for the three ions V^{2+}, Cr^{3+}, and Mn^{4+}. The theoretical values obtained from Eq. (26) are also given in Table III. The value of $[\Delta E/T_{z'z'}]$ used in Eq. (26) was originally measured in the case of Al_2O_3:Cr^{3+} by Schawlow[40] and more recently by Sturge[41] for the entire isoelectronic sequence and these values are listed in Table III. The other constants used in Eq. (26) are: $S_{33}-S_{13}=0.232\times10^{-12}$ cm^2/dyn [31] as given in Huntington's tables; $\rho=4$ g/cm^3; $v_l=10^6$ cm/sec, and $v_t\sim v_l/\sqrt{3}$. The reasonably good agreement between the theoretical and experimental values of $T_{2\bar{A}\to\bar{E}}$ in going from 12.3 to 80 cm^{-1} essentially verifies the Δ^3 dependence of the direct phonon process from $2\bar{A}$ to $\bar{E}$. The poorest agreement appears for the Mn^{4+} and is in the right direction to be explained by the dispersion in the ω versus k curve at 80 cm^{-1}, as the Debye acoustic limit is at $\approx$240 cm^{-1}. Since $T_{2\bar{A}\to\bar{E}}\sim v^5$, a dispersion that would reduce v by 20% at 80 cm^{-1}, would bring the results into more perfect agreement.

A few remarks can be made here about the absence of certain troublesome effects that occur in the usual measurement of spin-lattice relaxation by the pulse saturation technique. First, in a most general way, with the optical-detection technique, there is no danger that we might be measuring a spin diffusion time associated with "hole burning" rather than a true T_1. This is because by optical detection we monitor the recovery of the *total* population of a given level after the microwave saturating pulse is turned off and not the recovery of a particular spin packet. Thus, even if we do burn a hole in our microwave line, as indeed we believe we do as mentioned earlier, this will not influence our measurement of T_1. One still must be wary of cross-relaxation effects. However, as far as they are concerned we believe them to be minimal in the $\bar{E}$ state for the d^3 ions. For one, the splitting of $\bar{E}$ is sufficiently different from any of the $^4A_2$ ground-state splittings at the two microwave frequencies we used. Secondly, $g_\perp$ in $\bar{E}$ being very nearly equal to zero will also inhibit cross-relaxation. These factors make the $\bar{E}$ state of the d^3 ions an ideal system in which to study T_1.

ACKNOWLEDGMENTS

We wish to thank G. E. Devlin and M. B. Graifman for their experimental assistance during the course of this work, and Miss B. B. Cetlin for computational aid. We also wish to acknowledge the very many stimulating and helpful discussions with many of our colleagues, including M. Blume, A. Kiel, R. Orbach, and M. D. Sturge.

APPENDIX A

In discussing the hyperfine fields in the $\bar{E}$ state, care must be taken to properly interpret the sign of the electronic spectroscopic splitting factor, i.e., the g value. The lower of the Zeeman components of the $\bar{E}$ state labeled $(u_+-\frac{1}{2})$ (see Fig. 2) transforms as the Γ_4 double-valued representation of C_3, i.e., as $(+\frac{1}{2},+\frac{1}{2})$, while the upper Zeeman component $(u_-+\frac{1}{2})$ transforms as the Γ_5 double-valued representation of C_3, i.e., as $(+\frac{1}{2},-\frac{1}{2})$.[42] As the transformation properties of these levels is just opposite to that of normal electrons, transitions between them will be induced by resonant microwave radiation which is circularly polarized in an opposite sense to that which one associates with normal electron spins, as has been indicated earlier by Clogston.[43] Pryce[44] has pointed out that in axial sym-

---

[40] A. L. Shawlow, in *Advances in Quantum Electronics*, edited by J. R. Singer (Columbia University Press, New York, 1961), p. 50.

[41] M. D. Sturge (private communication).

[42] G. F. Koster, J. O. Dimmock, R. G. Wheeler, and H. Statz, *Properties of the Thirty-Two Point Groups* (M.I.T. Press, Cambridge, Massachusetts, 1963).

[43] A. M. Clogston, Phys. Rev. **118**, 1229 (1960).

[44] M. H. L. Pryce, Phys. Rev. Letters **3**, 375 (1959).

metry the sign of $g_{\parallel}$ determines the sense of precession of the magnetization so that in the spin Hamiltonian for the $\bar{E}$ state $g_{\parallel}$ should be taken as negative. The spin Hamiltonian including the hyperfine interaction and the nuclear Zeeman energy with H_0 along the c axis can be written as

$$\mathcal{H}=g_{\parallel}\beta S_z'\cdot H_0+A'm_I S_z'-g_I\beta_N m_I H_0,$$

where with $g_{\parallel}$ negative, S_z', the effective spin, is $+\frac{1}{2}$ for the lower Zeeman component and $-\frac{1}{2}$ for the upper Zeeman component. The hyperfine interaction constant A' referred to the fictitious spin S_z' would then have the opposite sign to its normal sense referred to the real electron spin. Therefore, note that although the sign of the hyperfine field in V^{2+} is the same in the excited $\bar{E}$ and ground $^4A_2$ states, the sign of A' in the $\bar{E}$ state is opposite to that given in the ground state because of the reversal between S and S'. However, the static magnetic properties of the $\bar{E}$ state as well as the sign of the magnetomechanical ratio $g'=2(mc/e)(\langle M_z\rangle/\langle J_z\rangle)$ correspond to that of normal electron spins, i.e., g' is positive. A fuller and more general treatment of g and g' is to appear in a forthcoming publication.[45] Thus, as far as hyperfine fields are concerned, one may speak of the core-polarization hyperfine field as having its normal negative sign referred to the real electron spin, i.e., it points in the direction of the real spin. Similarly, as far as calculating the orbital hyperfine field given by $H_{\mathrm{hf}}^{\mathrm{orb}}=+\Delta g_L 2\mu_\beta\langle 1/r^3\rangle$, one may regard $g_{\parallel}$ as *positive* and $\Delta g_L=|g_{\parallel}|-2$. To express this another way, the negative g value of -2.44 for Cr^{3+} is obviously *not* a result of $g_S=+2.0$ and $\Delta g_L=-4.44$; instead $\Delta g_L=+0.44$ and the negative $g_{\parallel}$ is simply used to describe the opposite sense of circular polarization needed to induce transition between $\bar{E}_-'$ and $\bar{E}_+'$.

APPENDIX B

We list in Table IV the one-electron product wave functions for the doublets of t_2^3 which were used to evaluate matrix elements of the dipolar operator a^z, the notation used is that of Griffith,[19] and Sugano and Tanabe.[9] The cubic vector coupling coefficients used to calculate these wave functions were taken from Tanabe and Kamimura.[46] The $S_z=-\frac{1}{2}$ state can be obtained from the given wave functions by operating on them with S_-.

TABLE IV. Wave functions of t_2^3 doublets, where the notation $t_i^2=t_i^+t_i^-$, $i=0$, $\pm$ has been employed.

$$|{}^2T_1,a_+ +\tfrac{1}{2}\rangle=(i/\sqrt{6})[\,|t_0^2t_+^+\rangle+2\,|t_-^2t_0^+\rangle-|t_+^2t_-^+\rangle]$$

$$|{}^2T_1,a_0+\tfrac{1}{2}\rangle=(i/\sqrt{6})[-|t_-^+t_+^-t_0^+\rangle+2\,|t_-^+t_+^+t_0^-\rangle+|t_+^+t_-^-t_0^+\rangle]$$

$$|{}^2T_1,a_- +\tfrac{1}{2}\rangle=(i/\sqrt{6})[-|t_0^2t_-^+\rangle+2\,|t_+^2t_0^+\rangle+|t_-^2t_+^+\rangle]$$

$$|{}^2T_2,x_+ +\tfrac{1}{2}\rangle=(1/\sqrt{2})[\,|t_0^2t_+^+\rangle+|t_+^2t_-^+\rangle]$$

$$|{}^2T_2,x_0+\tfrac{1}{2}\rangle=(-1/\sqrt{2})[\,|t_-^+t_+^-t_0^+\rangle+|t_+^+t_-^-t_0^+\rangle]$$

$$|{}^2T_2,x_- +\tfrac{1}{2}\rangle=(1/\sqrt{2})[\,|t_0^2t_-^+\rangle+|t_-^2t_+^+\rangle]$$

$$|{}^2E,u_+,+\tfrac{1}{2}\rangle=(1/\sqrt{3})[\,|t_-^2t_0^+\rangle-|t_+^2t_0^+\rangle-|t_+^2t_-^+\rangle]$$

$$|{}^2E,u_-,+\tfrac{1}{2}\rangle=1/\sqrt{3}[\,|t_0^2t_-^+\rangle+|t_+^2t_0^+\rangle-|t_-^2t_+^+\rangle]$$

The a_z matrix between the states of a single t_2 electron in a trigonal representation is given in Table V.

TABLE V. One-electron matrix elements of dipolar hyperfine-field operator a^z for t_2 orbital in a trigonal representation.

	t_+^+	t_+^-	t_0^+	t_0^-	t_-^+	t_-^-
t_+^+	-1					$2\sqrt{2}$
t_+^-		$+1$	$+\sqrt{2}/2$			
t_0^+		$+\sqrt{2}/2$	2			
t_0^-				-2	$-\sqrt{2}/2$	
t_-^+				$-\sqrt{2}/2$	-1	
t_-^-	$2\sqrt{2}$					$+1$

With these matrix elements and the wave functions in Table IV, one can verify that

$$\langle{}^2E,u_\mp\pm\tfrac{1}{2}\,|\,a^z\,|\,T_1,a_\mp\pm\tfrac{1}{2}\rangle=-\langle u_\mp\pm\tfrac{1}{2}\,|\,l^z\,|\,a_\mp\pm\tfrac{1}{2}\rangle$$
$$=\pm i\sqrt{2}.\quad\text{(B1)}$$

Assuming that these matrix elements are the major contributors to H^{dip} and Δg, respectively, leads to Eq. (19).

For the case of Mn^{4+} we also tried to include other matrix elements of a_z using a more exact wave function for the ^2E states obtained by diagonalizing the 16×16 matrix obtained within the manifold of the three doublets ^2E, $^2T_1$, and $^2T_2$. The values of the parameters used in Sugano and Tanabe's[9] notation were $K=-450$ cm^{-1}, $\zeta=230$ cm^{-1}, $k=1$; $W(^2T_2)-W(^2E)=6000$ cm^{-1}, $W(^2T_1)-W(^2E)=600$ cm^{-1}. The matrix elements of spin-orbit coupling and trigonal field are taken from Sugano and Tanabe,[9] and Tanabe and Kamimura.[46] The resulting wave function for $(\bar{E}u_+-\frac{1}{2})$ is given by

$$\bar{E}(u_+-\tfrac{1}{2})=(0.954)\,|u_+-\tfrac{1}{2}\rangle+(0.209)i\,|{}^2T_1,a_+-\tfrac{1}{2}\rangle$$
$$+(0.026)i\,|{}^2T_1,a_0+\tfrac{1}{2}\rangle-(0.210)\,|{}^2T_2,x_+-\tfrac{1}{2}\rangle$$
$$+(0.024)\,|{}^2T_2,x_0+\tfrac{1}{2}\rangle\quad\text{(B2)}$$

This wave function gives the correct splitting of 80 cm^{-1} between $\bar{E}$ and $2\bar{A}$ and also reasonably good values of $g_{\parallel}(\bar{E})=-3.114$ and $g_{\parallel}(2\bar{A})=1.142$. Using this wave function, we find that the extra matrix element $\langle{}^2E,\ u_+-\frac{1}{2}\,|\,a^z\,|\,{}^2T_1,\ a_0+\frac{1}{2}\rangle$ subtracts 14% from the value of $H_{\mathrm{hf}}^{\mathrm{dip}}$ given by Eq. (19) of the text. This is included, however, in the value of $H_{\mathrm{hf}}^{\mathrm{dip}}$ for Mn^{4+} in Table II.

---

[45] M. Blume, S. Geschwind, and Y. Yafet (to be published).

[46] Y. Tanabe and H. Kamimura, J. Phys. Soc. Japan **13**, 394 (1958).